UDK 539.42:669.018
Original scientific article/Izvirni znanstveni članek

ISSN 1580-2949
MTAEC9, 42(1)3(2008)

A FAILURE CRITERION FOR SINGLE-CRYSTAL SUPERALLOYS DURING THERMOCYCLIC LOADING

MERILO ZA PRELOM MONOKRISTALA SUPERZLITINE PRI TERMOCIKLIČNI OBREMENITVI

Leonid Getsov[1], Artem Semenov[1], Alexander Staroselsky[2]

[1]St. Petersburg State Polytechnical University, Russia, St. Petersburg, Polytechnicheskaja 29
[2]Pratt and Whitney, MS 165-16, East Hartford, CT, 06108 USA
guetsov@online.ru

Prejem rokopisa – received: 2007-09-12; sprejem za objavo – accepted for publication: 2007-12-18

The accumulation of deformation affects the lifetime of a monocristal submitted to low cyclic mechanical and thermal loading. An analytical method was developed considering the damages due to cyclic and axial plastic and creep deformation. The method was checked with tesst in vacuum on specimens of monocrystals with different space orientation, also specimens with stress concentrators. The distribution of stressses was FEM modelled. The fracture depends on the space orientation of the specimen and of the loading parameters. A new experimental-computational method using deformation-fracture criteria is suggested for the evaluation of the crystal life time

Keywords: single crystals,cyclic and axial loading, thermal fatigue, failure criteria

Kopičenje deformacije vpliva na trajnostno dobo kovine, ki prenaša malociklično mehansko in termično obremenitev. Razvita je bila analitična metoda, ki sešteva poškodbe zaradi cikličnih in enoosnih plastičnih deformacij in deformacije z lezenjem. Metoda je preverjena s preizkusi v vakuumu na vzorcih monokristalov z različno prostorsko orientacijo. Preizkusi so bili izvršeni tudi z vzorci z obliko, ki je povzročala lokalno koncentracijo napetosti. Porazdelitev napetosti je bila modelirana po metodi končnih elementov. Prelom je odvisen od prostorske orientacije in od parametrov obremenitve. Predlagana so nova deformacijsko-prelomna merila za oceno trajnostne dobe monokristala na podlagi eksperimentalno-računske analize.

Ključne besede: monokristali, ciklična in aksialna obremenitev, termična utrujenost, pogoji za prelom

1 INTRODUCTION

The deformation criterion

$$D_1(\Delta\varepsilon_{pl_i}) + D_2(\Delta\varepsilon_{c_i}) + D_3(\varepsilon_{pl_i}) + D_4(\varepsilon_{c_i}) = 1 \qquad (1)$$

for the fracture of metal in conditions of low-cycle and thermal-cycle loading was proposed in [1]. The quantitative result of the lifetime test on the basis of this criterion depends on the choice of the deformation parameters.

The proposed deformation criterion is based on the summation of the damage caused by cyclic plastic deformations $D_1 = \frac{1}{C_1}\sum_n (\Delta\varepsilon_i^{pl})^k$, cyclic creep deformations $D_2 = \frac{1}{C_2}\sum_n (\Delta\varepsilon_i^{pl})^k$, unilaterally accumulated plastic deformations $D_3 = \frac{1}{C_3}\sum_n \frac{\varepsilon_i^{pl}}{\varepsilon_r}$ and unilaterally accumulated creep deformations $D_4 = \frac{1}{C_4}\sum_n \frac{\varepsilon_i^{pl}}{\varepsilon_r}$.

In the case of interference of the above-mentioned types of damage the relevant corrections are made by considering the limiting characteristics of the material, C_1, C_2, ε_r, and ε_{cr}. This criterion was tested experimentally under conditions of uniaxial and composite tension for various samples, and the GTE details made of isotropic heat-resistant steels and alloys that fracture are caused by low-cycle or thermal fatigue (see **Figure 1** and [2–4 and others]).

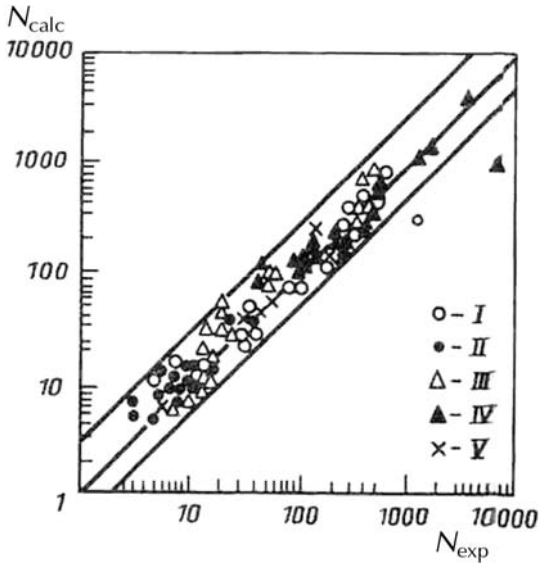

Figure 1: The correlation between the experimental and calculated values of the lifetime: I-D_1+D_2, II-D_3+D_4, III-D_1+D_2+D_4, IV-D_1+D_3 +D_4, V-D_1+D_2+D_3 +D_4

Slika 1: Korelacija med eksperimentalnimi in izračunanimi vrednostmi za trajnostno dobo I-D_1+D_2, II-D_3+D_4, III-D_1+D_2+D_4, IV-D_1 +D_3+D_4, V-D_1+D_2+D_3+D_4

The quantitative result of the details' lifetime test on the basis of this criterion depends on the choice and precision of its deformation parameters. As for the isotropic materials, normally the role of such parameters is played by the intensities of the total amplitudes of the deformations

$$\Delta\varepsilon_i^{pl} = \sqrt{\frac{2}{9}\left[(\Delta\varepsilon_1^{pl} - \Delta\varepsilon_2^{pl})^2 + (\Delta\varepsilon_2^{pl} - \Delta\varepsilon_3^{pl})^2 + (\Delta\varepsilon_3^{pl} - \Delta\varepsilon_1^{pl})^2\right]} \quad (2a)$$

$$\Delta\varepsilon_i^{c} = \sqrt{\frac{2}{9}\left[(\Delta\varepsilon_1^{c} - \Delta\varepsilon_2^{c})^2 + (\Delta\varepsilon_2^{c} - \Delta\varepsilon_3^{c})^2 + (\Delta\varepsilon_3^{c} - \Delta\varepsilon_1^{c})^2\right]} \quad (2b)$$

and the intensities of the accumulated deformations,

$$\varepsilon_i^{pl} = \sqrt{\frac{2}{9}\left[(\varepsilon_1^{pl} - \varepsilon_2^{pl})^2 + (\varepsilon_2^{pl} - \varepsilon_3^{pl})^2 + \varepsilon_3^{pl} - \varepsilon_1^{pl})^2\right]} \quad (3a)$$

$$\varepsilon_i^{c} = \sqrt{\frac{2}{9}\left[(\varepsilon_1^{c} - \varepsilon_2^{c})^2 + (\varepsilon_2^{c} - \varepsilon_3^{c})^2 + (\varepsilon_3^{c} - \varepsilon_1^{c})^2\right]} \quad (3b)$$

In this research we studied the possibility of generalizing the above-mentioned criterion for the case of single-crystal alloys. This generalization was based on the following relationships for fatigue-crack initiation and growth in the references [5–12].

According to the experimental data, the increase of temperature [5] and the reduction in the of frequency [6] change the mechanism of fracture in single crystals, which means that the transition from crack growth along ***crystallographic*** (octahedral) planes to growth in other directions does not depend on the crystal orientation, but on the conditions of loading (according to ***Mode* I**). The non-crystallographic growth is observed predominantly on the boundary of the γ/γ' phases.

One of the possible explanations [20] for such a transition is the initiation of additional damage owing to the influence of the environment. Oxygen-related brittle behavior in the vicinity of the crack tip takes place according to the diffusion mechanism, and is sensitive to the temperature, the time (frequency) and the concentration of oxygen. A comparison of the results of the experiments made in air [5] and in vacuum [7] has shown that the transition temperature is considerably higher in vacuum. When the frequency is decreased, the time of the brittle behavior within the cycle increases, which promotes the further penetration of oxygen, and this initiates the transition from the crystallographic mode of crack growth to the non-crystallographic mode I. Also, the increase in the temperature accelerates the diffusion process, promoting the transition from a crystallographic to a non-crystallographic mechanism of crack growth.

As shown in [8], the threshold value for non-crystallographic fractures, ΔK_{thI}, is lower than the value of $\Delta K_{th(111)}$ for cracks growing along a crystallographic plane, and when ΔK_{eq} becomes lower than $\Delta K_{th(111)}$ the crack cannot continue growing according to the crystallographic mechanism and goes over to growth according to mode I. Thus, the experiments show that the transition from the crystallographic to the non-crystallographic stage is controlled by the temperature T, the frequency f, and the total amplitude of SIF, ΔK.

For the set of above-mentioned parameters it is possible to create maps of mechanisms for the growth of fatigue cracks (analogous to the maps for static loading in [9], showing the boundaries between the crystallographic and non-crystallographic areas of crack growth). As an example of such a map, the reader is referred to the map in [10] (see **Figure 2**), obtained on the basis of an examination of thermally activated slip processes in the vicinity of the crack tip.

The transition from the crystallographic mode of growth at high temperatures is also promoted by the decrease in the anisotropy of the elastic and strength characteristics of crystals. So, at high temperatures (≈980 °C) the growth rate of the fatigue cracks does not, in practice, depend [11] on the orientation of single crystals under the conditions of a uniaxial and composite deformation mode. This probably explains the absence of anisotropy in high-temperature multi-cycle fatigue.

It is important to note that the arborescent structure also influences the change of the orientation of the fatigue-crack growth and it could provoke the transition from one crystallographic plane to another. The equalization of the crack-growth rates for single crystals with orientations [111] and [001] can be explained [1,11,12] by the fact that as ΔK grows, the fatigue-crack trajectory diverts from the plane (111) perpendicular to the loading axis and evolves into the plane (001), where inter-dendrite areas are concentrated, i.e., to the same plane in which the fatigue cracks grow in samples with the orientation [001].

As a two-dimensional model, interpreting simply the fatigue crack's growth in the area surrounding the cooling duct, the problem of crack growth in a plate with

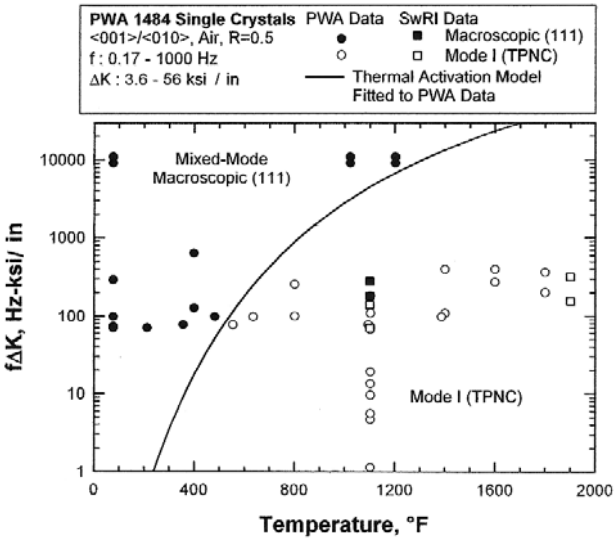

Figure 2: Map of fatigue-crack growth mechanisms for monocrystals <001>/<010> PWA 1484 [10]

Slika 2: Shema mehanizma rasti utrujenostne razpoke za monokristale <001>/<010> PWA 1484 [10]

a circular hole can be considered. The plate is in non-uniform temperature conditions with the minimum value of the temperature on the edge of the hole: the greater is the distance from the hole, the higher are the temperature and the SIF. The crack-growth process on the plane of parameters corresponding to the map of mechanisms of fatigue-crack growth in a single crystal is shown schematically in **Figure 5** with the line ABC. When the boundary between the crystallographic and non-crystallographic stages is crossed at the point B, the crack changes its growth direction. With the change in the mechanism and the direction of the crack growth, the speed of growth also changes.

Depending on the load level and the frequency, the sample orientation, the geometrical parameters of the plate with a hole and the material properties, different schemes of crack growth are possible. Among them are both the modes without a direction change (in one plane, crystallographic or non-crystallographic) and modes with one or multiple direction changes.

The extrapolation of the research results described in [12] for the conditions of thermal-cycle loading and, as a final goal, the development of a new fracture criterion, have become the object of the present research. At the same time, we are not discussing here the problems of the choice of models for the visco-elastic plasticity for the calculation of parameter values of criterion (1).

2 TEST METHODS

The thermal fatigue tests were performed for samples made of a single-crystal high-temperature alloy with five different orientations, including <001>, <011> and <111>. During the tests, the samples in sand-glass form were rigidly fixed in vacuum [13].

A comprehensive procedure is developed in NPO CKTI for the definition of the thermal fatigue resistance of various materials and coatings, applying a special appliance that allows us to clamp flat the sand-glass shaped test pieces and to ensure their cyclic heating with a conducting current (**Figure 3**). The heating takes place according to a specified program (**Figure 4**), maintained automatically during the testing. The appliance is fixed in a vacuum chamber. The ultimate cycle temperature, defined by the rate of oxide-film formation on the sample surface, increases with the vacuum. The sample material's behavior at various surface points on the sample is observed using a microscope with a 250× magnification. During the test the following parameters are recorded: the characteristic properties of the deformation relief defining the mechanism of the accumulation of thermal fatigue damage; the number of cycles to the first microcrack formation in various elements of the metal and the coating; the growth rate of the incipient cracks; the number of cycles to sample failure and the accumulated deformations in the ruptured zone.

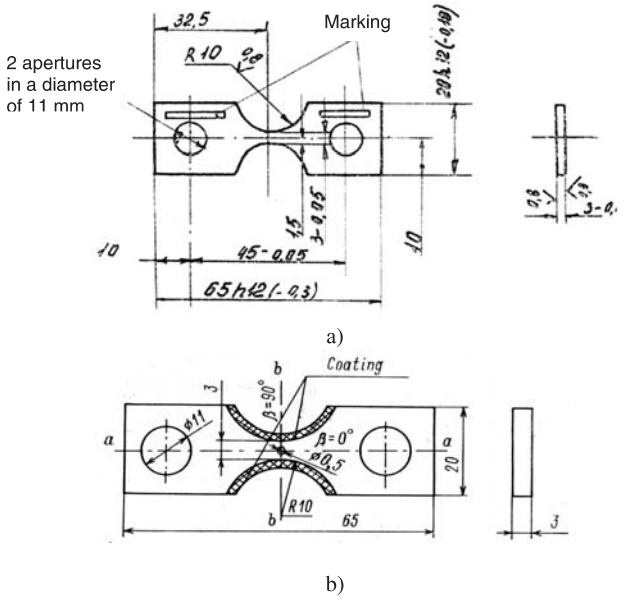

Figure 3: Shape of the specimen (a) and a sketch of the specimen with a coating and with a central hole (b)
Slika 3: Oblika preizkušanca (a) in shema preizkušancev s prekritjem in z osrednjo izvrtino (b)

The range of the conditionally elastic stresses $\Delta\sigma$ and the range of the total deformation $\Delta\varepsilon$ in the specimen's working part in the cycle were calculated from thee equations:

$$\Delta\sigma = (E_{st1}\alpha_1 T_{max} - E_{st2}\alpha_2 T_{max})\varphi$$
$$\Delta\sigma = (\alpha_1 T_{max} - \alpha_2 T_{max})\varphi \quad (4)$$
$$\varphi = 1 - \Delta k / \Delta l$$

where E_{st} is the static elastic modulus; Δl is the free travel of the test points during heating from $T_{mi\ n}$ to T_{max}; and Δk is the measured value of the displacement of the control microhardness marks, applied to the sample surface along its working-part edges during the cycle.

In this calculation the values Δk and φ were used after being averaged on the basis of the hypotheses of their linear summability.

Some 9-mm-wide plates of a single-crystal alloy with different orientations were prepared for the tests (see **Table 1**).

Table 1: Sample orientation
Tabela 1: Orientacija preizkušancev

Number of the sample series	Orientation	Deviation from the exact axial orientation in degrees	Azimuthal orientation of the crystallo-graphic planes in degrees
1	111	5.64	8.26
2	011	4.51	11.27
3	011	8.33	14.43
4	011	9.67	7.86
5	001	5.47	41.97

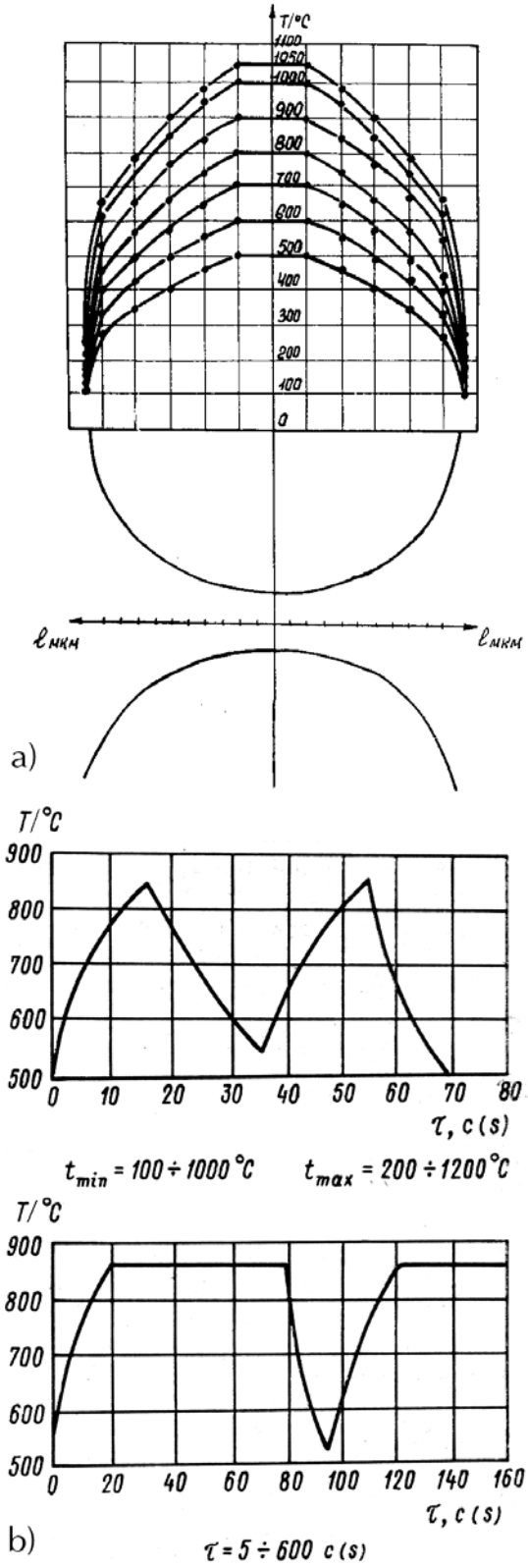

Figure 4: Experimentally determined distribution of the temperature along the length of the sample (à) and an example of the change of the maximum temperature in the working part of the sample during the cycle (b)

Slika 4: Eksperimentalno določena porazdelitev temperature po dolžini preizkušanca (a) in primer spremembe najvišje temperature v delovnem delu preizkušanca med ciklom (b)

Some tests were made on samples with stress concentrators in the form of holes with a diameter of 0.5 mm. The tests were conducted under different maximum temperatures in the cycle T_{max} (850–1050 °C) with and without 2–5 min of holding at $T_{max.}$ The positions of the slip lines on the sample's surface were calculated and confirmed experimentally, as was the crack orientation up to the moment of the sample's rupture. The values of the irreversible deformations (characterizing the ratcheting) taking place in the central part of the samples were also determined.

For the interpretation of the test results we: a) analyzed the character of the fracture from the four sides of the sample (see **Figure 5**) and b) carried out finite-element calculations for the change of the sample's deformation mode in order to find the orientations of the rupture surfaces with the help of methods for deformable solid-body mechanics and to compare the results with crystallographic predictions and experimental data.

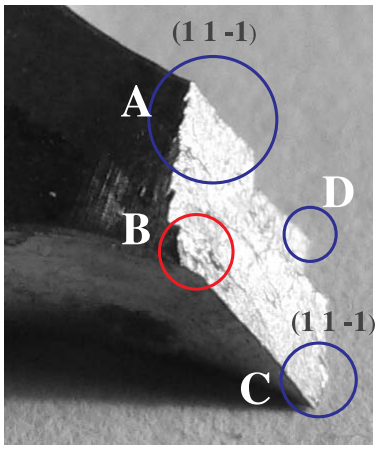

sample 3-2

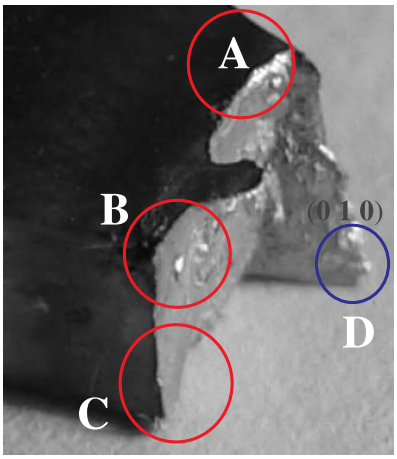

sample 3-5

O – Crystallographic fracture, O – Non-crystallographic fracture.

Figure 5: Interpretation of the fracture character of the samples 3-2 and 3-5

Slika 5: Interpretacija značilnosti preloma preizkušancev 3-2 in 3-5

3 EXPERIMENTAL RESULTS AND THEIR ANALYSIS

The results of the performed experiments were compared to the results of the crystallographic analysis and the calculation of the samples' deformation mode. The stress analysis of the samples was performed with the help of the PANTOCRATOR finite-element program [14] (see http://www.pantocrator.narod.ru) based on the following assumptions:

1) in the tension phase, the cleavage cracks can originate and grow, and their growth direction is determined by the orientation of the platform of the maximum principal value of the stress tensor,
2) in the compression phase, the shear cracks can originate and grow, and their growth direction is determined by the orientation of the platforms of the maximum tangent stresses.

From now on the concept of non-crystallographic fracture mode is used in the phenomenological context, as a fracture (observed at the macro-level) not coinciding with any of the crystallographic slip planes.

As an example, let us consider the place of origin of a shear crack on the basis of the hypothesis of maximum tangential stresses for a sample of the 3rd group tested in the mode 150–900 °C. We found that there are two equal, centrally symmetric maximums τ_{max} = 856 MPa with a bias located at a distance of 0.64 mm from the center (see **Figure 6**), and the stresses localized in the lateral zones (with a maximum on the center line) (see **Figure 6b**).

For the same sample, we identified the tensile-crack initiation point using the hypothesis of maximum principal stresses. We found that there are two equal, centrally symmetric maximums σ_1 = 1559 MPa at a distance of 0.45 mm from the centre (see **Figure 7**); there is also a localization of stresses in the lateral zones (with a maximum at the edge) (see **Figure 7b**).

An analysis of the calculation results showed that the distribution of stresses σ_x and the locations of the maximum stress zones are very different for different groups of samples.

An example of the experimental data analysis is shown in **Table 2**, containing the results for sample 2-1 tested under the mode 150–900 °C.

For this sample the crystallographic and the finite-element results are similar and show only an insignificant difference compared to the experiment (a

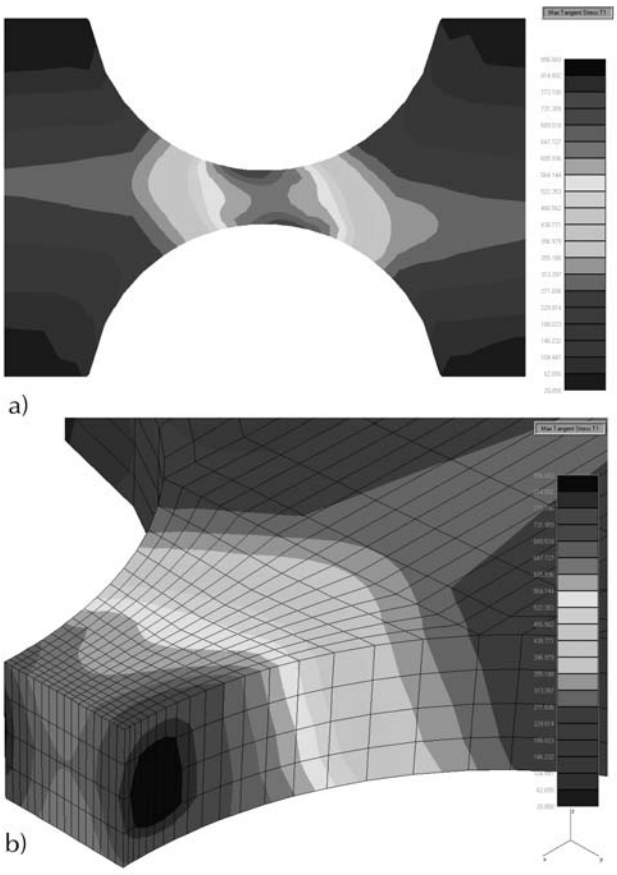

Figure 6: Distribution of the fields of maximum tangential stress (sample 3-0, 3rd cycle)

Slika 6: Porazdelitev polj največjih tangencialnih napetosti (preizkušanec 3-0, 3. cikel)

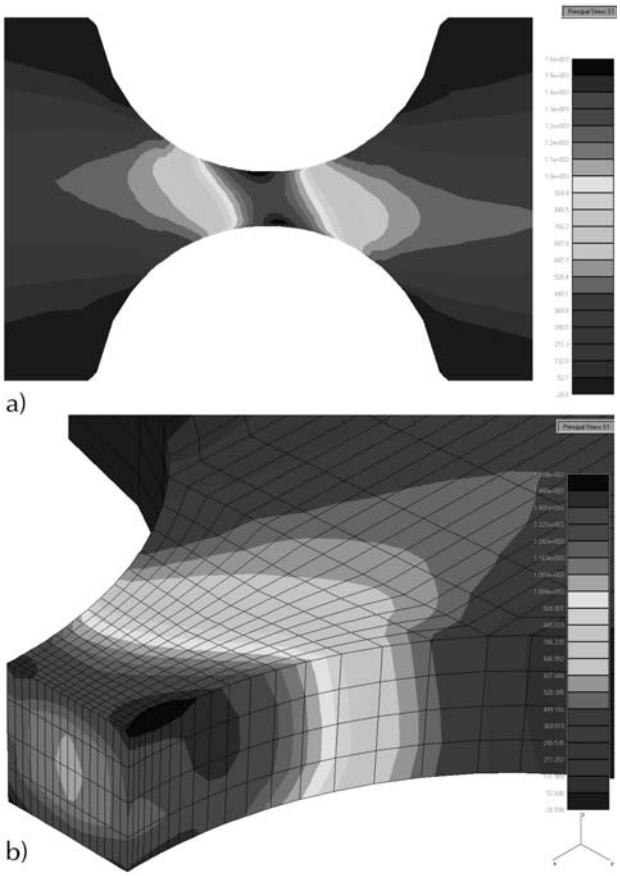

Figure 7: Distribution of fields of maximum principal stress (sample 3-0, 3rd cycle)

Slika 7: Porazdelitev polj največjih glavnih napetosti (preizkušanec 3-0, 3. cikel)

Table 2: Comparison of the experimental data with the results of the crystallographic and finite-element analyses of specimen 2-1
Tabela 2: Primerjava eksperimentalnih podatkov in rezultatov kristalografske analize in analize po metodi končnih elementov za preizkušanec 2-1

	Expe-riment	crystallography	FEA	
			cleavage mode	shear mode
A	84 / 49	84 / 51 (1-11)	90 / 90	88 / 45
B	90 / 47	84 / 51 (1-11)		
C	86 / 49	84 / 51 (1-11)		
D	86 / 49	84 / 51 (1-11)		

maximum of 4°). Symbolically, we designate fractures of this type as "Mode 90 / 45".

Owing to the absence of pure modes of crystallographic or non-crystallographic fracture and, in some cases, to the ambiguities of the choice between the modes caused by the neighboring prognoses of the crystallographic and the finite-element analysis, in order to map the fracture mechanisms we use the classification of modes on the basis of the orientation of the middle fracture "plane" instead of the concepts of crystallographic or non-crystallographic fracture modes the four modes are considered:

- Mode 90 / 45
- Mode 90 / 90

} crystallographic or SSS

- Mode 45 / 45
- Mode 45 / 90

} crystallographic

In **Table 3** the results of the analyses of the fracture modes for the samples from group 3 are shown. The results show that the sample's rupture occurred in the

Table 3: Dominant fracture modes of the samples of the 3rd group (τ-duration of cycle)
Tabela 3: Prevladujoči načini preloma preizkušanca iz 3. skupine (τ-trajanje cikla)

Sample	T_{min}/ ^{0}C	T_{max}/ ^{0}C	τ/s	N	$\Delta\varepsilon$/%	Isometric view	Front view	Side view	Mode
3-0	150	900	80	951	0.77			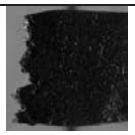	90/90 (Non-Crystal)
3-1	200	950	60	450	0.88			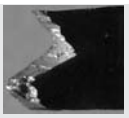	90/45 (Crystal)
3-2	250	1000	64	63	0.68			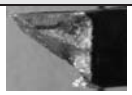	90/45 (Crystal)
3-3	500	1000	25	1220	0.68	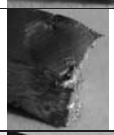	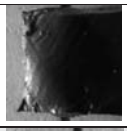	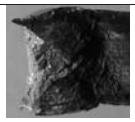	90/45 (Crystal)
3-4	550	1050	23	356	0.41				90/45 (Crystal)
3-5	450	950	20	2535	0.49		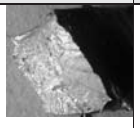		90/90 (Non-Crystal)
3-0	150	900	80	951	0.77				90/90 (Non-Crystal)
3-1	200	950	60	450	0.88				90/45 (Crystal)

Non-FE, non-forecasting with the finite-element analysis

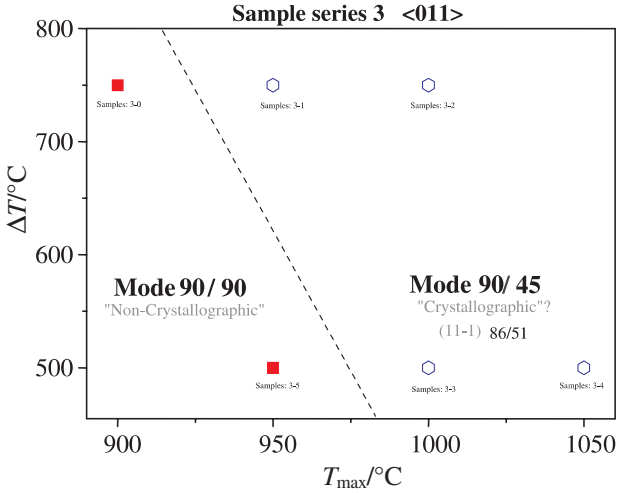

Figure 8: Map of the fracture mechanisms for the samples of the 3rd series

Slika 8: Shema mehanizma preloma za preizkušance iz 3. serije

crystallographic, the non-crystallographic and the mixed modes. The conditions for the occurrence of the crack type (dominant type (mode) of fracture) are generalized with the help of maps of fracture mechanisms plotted in the coordinates $T_{MAX} - \Delta T$ (see, for example, **Figure 8**). With the help of such maps of fracture mechanisms it is possible to separate the loading conditions.

Fracture criterion. The above-mentioned facts make it evident that, depending on the fracture mode of single-crystal alloys, in each concrete case it is necessary to choose the corresponding deformation-fracture criteria:

- criterion 1:

$$D_1(\Delta\gamma_{pl}) + D_2(\Delta\gamma_c) + D_3(\gamma_{pl}) + D_4(\gamma_c) = 1 \qquad (4)$$

- criterion 2

$$D_1(\Delta\varepsilon_{pl1}) + D_2(\Delta\varepsilon_{c1}) + D_3(\varepsilon_{pl1}) + D_4(\varepsilon_{c1}) = 1 \qquad (5)$$

Namely, for crystallographically oriented fracture modes, the following criterion parameters must be chosen: shear deformations and their total amplitudes γ_{pl} and $\Delta\gamma_{pl}$ (γ_c, $\Delta\gamma_c$), and for non-crystallographic fracture modes, the tensile deformations and their total amplitudes ε_{pl1}, $\Delta\varepsilon_{pl1}$, ε_{c1}, and $\Delta\varepsilon_{c1}$.

Let us take as a basis the fact that the performed thermal fatigue tests are described, on the one hand, by the total number of cycles and, on the other hand, by the level of the ratcheting deformation.

Table 4: Comparison of the ratcheting deformation ε_{max} with the thermal fatigue and plasticity (short-time plasticity ε_r and creep-rupture plasticity ε_{cr}) at high temperature

Tabela 4: Primerjava prelomnih deformacij ε_{max} s termično utrujenostjo in plastičnostjo (kratkotrajna plastičnost ε_r in plastičnost pri prelomu z lezenjem ε_{cr}) pri visoki temperaturi

Orientation	T_{max}/°C	Time of stay, min	ε_{max}/%	ε_{max1}/ ε_{max2}	N	N_2/N_1	ε_r % at T_{max}	ε_{cr} % at T_{max}	D_3	D_4
001	900	0	9.0	0.75	560	0.17	27	12.8–16.4	0.1	0
	1000	0	12		95		19	8–23	0.25	0
111	900	0	10.7 24.3*		823 50		19,5	14–24	0.22 0.5	0
		2	21		140				0	0.35–0.6
		5	18.3		16				0	0.3–0.52
	1000	2	23.7		194		21,5	7.2–23.8	0	0.4–1.3
011(2)	850	0	9.3*		2952					
	900	0	15.3		100					
	1000	0	20	0.67	472	0.67				
		5	29.7		317					
		0	10.6*	0.77	187	0.33				
		2	13.7*		62					
011(3)	900	0	10.3		951					
	950	0	4.3	0.4	2535	0.18				
	950	0	10.7		450					
	1000	0	7.3	0.6	1220	0.05				
	1000	0	12		63					
	1050	0	14.7		356					
011(4)	900	0	10	0.47 0.55	308	0.06 0.08				
	900	2	21.3		17					
	900	5	18		26					
	900	0	9.7*		25					
	950	0	9.7	0.94	626	0.20				
	950	2	10.3		128					

*-specimen with concentrator

Table 5: Calculation of damage by means of (5)
Tabela 5: Izračun poškodb z uporabo (5)

Orientation	The minimum temperature of a cycle, °C	The maximum temperature of a cycle, °C	Time of cycle, sec	Number of cycles before formation of the main crack, N_m	$\Delta\varepsilon$ %	$2\sigma_{-1}/E$	$\Delta\varepsilon_{el}$ %	$\Delta\varepsilon_{pl,c}$ %	D_1	D_2	D_3	D_4	ΣD_i
[111]	150	900	72	190	0.73	$860/2.4\cdot10^5$	0.36	0.37	0.273	0	0.22	0	0.59
			247	50	0.69	$860/2.4\cdot10^5$	0.36	0.33	0	0.34	0	0.35	1.27
			378	12	0.73	$860/2.4\cdot10^5$	0.36	0.37	0	0.09	0	0.52	0.61
	500	1000	149	80	0.64	$648/2.3\cdot10^5$	0.28	0.36	0	0.60	0	0.40	1.00
[001]	150	900	72	500	0.86	$700/0.998\cdot10^5$	0.70	0.16	0.013	0	0.10	0	0.11
	250	1000	48	40	0.855	$500/0.95\cdot10^5$	0.52	0.33	0.18	0	0.25	0	0.43
	500	1000	28	1400	0.655	$500/0.95\cdot10^5$	0.52	0.13	1.13	0	0.25	0	1.38

The data in **Table 4** show that a) a decrease of the ratcheting deformation results in a sample lifetime increase, b) the number of cycles to fracture in tests with holding at T_{MAX} is considerably lower than the numbers of cycles in the case of tests without such holding. The research of Sizova R.N.[15] has shown that, in conditions of compression, the time to fracture is 2.5–3.0 times longer than in the case of tension. Using the deformation criterion of destruction, it is equivalent to the updating of the ratio $D_3 = \varepsilon_{max}/\varepsilon_r$ and $D_4 = \varepsilon_{max}/\varepsilon_{cr}$, with the help of the correction factor 0.4. We then have:

$$D_3 = 0.4\ \varepsilon_{max}/\varepsilon_r \quad (6)$$

$$D_4 = 0.4\ \varepsilon_{max}/\varepsilon_{cr} \quad (7)$$

where ε_r and ε_{cr} are the corresponding deformations in the case of short-time fracture and fracture in the creep test at T_{MAX} under tension.

Let us compare the deformations ε_{max} for two tests, ε_{max1} and ε_{max2}. We can see that the relation ($\varepsilon_{max1}/\varepsilon_{max2} - N_2/N_1$) varies from 0.12 up to 1.00. This means that the ratcheting deformation value cannot characterize the fracture conditions and only helps to identify the trend.

Here are $\varepsilon_{max} = \max(\varepsilon_1, \varepsilon_2)$, where ε_1 and ε_2 are the deformations measured in two directions of the sample's cross-section.

To apply the proposed deformation criterion (1) to the results of the performed tests it is necessary: a) to calculate appropriately (using creep parameters and deformation curves in conditions of short-time tension) the width of the hysteresis curve, with reference to the known temperature-change graph, b) to have the values of the short-time and long-time plasticity at T_{MAX}. A comparison of the single-crystal alloy plasticity values ε_r obtained during the simple tension tests and the ε_r in long-term tests prove that, like for polycrystalline materials, in creep conditions the plasticity of the material is less than the short-time plasticity.

Having the experimental values of ratcheting deformations and supposing that the exponents in the expressions for D_1 and D_2 are equal to 2.0 and 1.25 (like in the case of polycrystalline materials), the calculation of the number of cycles until fracture turns out to be dependent on the two material parameters and the maximum temperature in the cycle. As a first approximation, these material parameters can be evaluated from the values ε_r and ε_{cr} ($C_1 = (0.5\varepsilon_r)^2$, $C_2 = (0.75\ \varepsilon_{cr})^{1,25}$).

Let us consider some results of the calculation of the interruption mechanism damage. The calculation of the damage D_1 and D_2 (see **Table 5**) was carried out with reference to the number of cycles before the occurrence of the main crack, N_m. The size of the range of the non-elastic deformation $\Delta\varepsilon_{pl}$ and $\Delta\varepsilon_c$ was determined as the difference of the range of full deformations, $\Delta\varepsilon$, and the sizes $2\sigma_{-1}/E$. Thus, it was accepted that the cyclic limit of the elasticity is equal to the fatigue strength at the maximum temperature of the cycle. For the calculation the D_1 and D_2 values of plasticity were accepted under a simple tension (ε_r) and at the long rupture time (ε_{cr}) given in **Table 6**. The values of the damage D_3 and D_4 are calculated by means of Equations (6) and (7) and the experimentally obtained values of ratcheting and plasticity during compression. The data in Table 5 confirm the satisfactory description of the conditions of the origin of the main cracks found during thermocyclic loading of a single-crystal alloy.

Table 6: Input data
Tabela 6: Vhodni podatki

Temperature/ °C	Elongation (ε_r)/%		Long time elongation (ε_{cr})/%		Fatigue limit σ_{-1}/MPa		
	[001]	[111]	[001]	[111]	[001]	[011] approximately	[111]
900	27	19.5	8.6–16.4	14.1–24	350	360	430
1000	19	21.5	8–23	7.2–23.8	–	–	–
1100	22	21.5	–	–	170	170	170

Table 7: Relations between the shear strain γ_{nl} and the axial strain ε_x
Tabela 7: Razmerje med strižno deformacijo γ_{nl} in axialno deformacijo ε_x

Specimen series	Specimen orientation	$\gamma_{nl}/\varepsilon_x$
1.	[111]	4.25
2.	[011]	4.50
3.	[011]	4.09
4.	[011]	2.80
5.	[001]	2.16

Shear-strain computation. The criterion (4) requires a shear-strain ($\Delta\gamma_{pl}$, $\Delta\gamma_c$, γ_{pl}, and γ_c) computation. The shear strain γ_{nl} at the plane with the normal vector $\boldsymbol{n}$ in the slip direction $\boldsymbol{l}$ is defined on the basis of the strain tensor ε by the relation

$$\gamma_{nl} = 2\varepsilon_{nl} = 2\boldsymbol{n}\cdot\varepsilon\cdot\boldsymbol{l} \tag{8}$$

or, by using a presentation with components

$$\begin{aligned}\gamma_{nl} = 2\varepsilon_{nl} = 2(&n_x\varepsilon_{xx}l_x + n_x\varepsilon_{xy}l_y + n_x\varepsilon_{xz}l_z + \\ &+n_y\varepsilon_{xy}l_x + n_y\varepsilon_{yy}l_y + n_y\varepsilon_{yz}l_z + \\ &+n_z\varepsilon_{xz}l_x + n_z\varepsilon_{yz}l_y + n_z\varepsilon_{zz}l_z)\end{aligned} \tag{9}$$

The presented equations are valid for all cases, $\Delta\gamma_{pl}$, $\Delta\gamma_c$, γ_{pl} and γ_c, with a special choice of the strain tensor for each case.

The components of the normal vector $\boldsymbol{n}$ and the slip direction $\boldsymbol{l}$ in the global coordinate system are related to the components in the crystallographic coordinate system by the following relations

$$\begin{aligned}n_x &= A_{11}n_{<100>} + A_{21}n_{<010>} + A_{31}n_{<001>} \\ n_y &= A_{12}n_{<100>} + A_{22}n_{<010>} + A_{32}n_{<001>} \\ n_z &= A_{13}n_{<100>} + A_{23}n_{<010>} + A_{33}n_{<001>}\end{aligned} \tag{10}$$

and

$$\begin{aligned}l_x &= A_{11}l_{<100>} + A_{21}l_{<010>} + A_{31}l_{<001>} \\ l_y &= A_{12}l_{<100>} + A_{22}l_{<010>} + A_{32}l_{<001>} \\ l_z &= A_{13}l_{<100>} + A_{23}l_{<010>} + A_{33}l_{<001>}\end{aligned} \tag{11}$$

where A_{ij} is the matrix of crystallographic orientations, which is different for each specimen.

The results of the computations of γ_{nl} for all the specimen series are given in **Table 7**. The diagonal components of the strain tensor are obtained from the experimental data and the non-diagonal components are taken from the finite-element simulations.

The results of the calculation of damage with the use of criterion (4) are shown in **Table 8**.

For the definition of the damage size the following relations were used:

$$\begin{aligned}&D_1 = \frac{1}{C_3}\sum_n(\Delta\gamma_i^{pl})^k;\ D_2 = \frac{1}{C_4}\sum_n(\Delta\gamma_i^{pl})^k; \\ &D_3 = 0.4\gamma_{max}/\gamma_r;\ D_4 = 0.4\gamma_{max}/\gamma_{cr}\end{aligned} \tag{12}$$

where the values of the constants C_3, C_4, γ_r, and γcr were defined using the ratio

$$C_3 = 2.25\ C_1;\ C_4 = 1.66\ C_2;\ \gamma_r = 1.5\ \varepsilon_r;\ \gamma_{cr} = 1.5\ \varepsilon_r \tag{13}$$

For the orientation [111], the sum of the damage agrees with the criterion (4) at the moment of formation of the main crack, and appears to be much more than 1.0, while calculations that use this criterion (5) are in good agreement with the experiment. Thus, criterion (4) gives, in this case, an underestimated number of cycles. At the same time the use of this criterion for two samples with the orientation [001] gives the best agreement with the experiment in comparison to criterion (5), and for one specimen the agreement is worse.

The use of diagrams of maps of destruction (see **Figure 8**) allows us to predict the criterion of destruction during the thermal cyclic loading of objects made from single-crystal alloys.

The use of the forgoing modification of the deformation fracture criterion will make it possible to solve reliably the problems of the prediction of the conditions of initiation of the thermal-fatigue cracks in the turbine blades made of single-crystal alloys.

4 CONCLUSIONS

The performed experimental investigation and the analysis led to the following conclusions:

1. The character of fracture of single-crystal alloys under thermal-cycle loading depends on the crystallographic orientation of the material and on the

Table 8: Calculation of damages by means of (4)
Tabela 8: Izračun poškodb z uporabo (4)

Orientation	The minimum tempera ture of a cycle, °C	The maximum temperature of a cycle, °C	Time of cycle, s	Number of cycles before formation of the main crack, N_m	$\Delta\gamma_{pl,c}$ %	$D_1(\Delta\gamma_{pl})$	$D_2(\Delta\gamma_c)$	$D_3(\gamma_{pl})$	$D_4(\gamma_c)$	ΣD_i
[111]	150	900	72	190	1.57	2.19	0	0.62	0	2.81
			247	50	1.40	0	3.6	0	0.99	4.59
			378	12	1.57	0	0.16	0	1.47	1.63
	500	1000	149	80	1.53	0	11.7	0	1.13	12.83
[001]	150	900	72	500	0. 345	0.027	0	0.144	0	0.171
	250	1000	48	40	0.71	0.37	0	0.36	0	0.73
	500	1000	28	1400	0.28	2.34	0	0.36	0	2.70

temperature and time parameters of the loading mode.

2. The difference of the fracture mechanisms for each case of crystallographic orientation of the material can be represented with the help of the proposed fracture maps using the coordinates T_{MAX} $-\Delta T$.
3. New definitions for the deformation fracture criteria of single-crystal alloys in conditions of thermal-cycle loading have been proposed; they make it possible to evaluate the lifetime of blades made of single-crystal alloys using a computational-experimental approach.

In summary, the use of the deformation criterion for the calculation of fracture conditions for single-crystal alloys submitted to thermal-cycle loading requires, on the one hand, a knowledge of the creep and plasticity characteristics of the material for different crystallographic orientations in the working temperature range, and, on the other hand, the appropriate choice of the thermo-visco-elasto-placticity model.

5 REFERENCES

[1] L. B. Getsov: Problems of creation of the "universal" theory of destruction of materials. Journal of machinery manufacture under reliability problem. (**2001**) 5, 49–55

[2] K. M. Kononov, L. B. Getsov: Failure criteria of materials under cyclic loading. Strength of materials, N2, 1984

[3] P. A. Pavlov, L. B. Getsov: Deformation criteria for material rupture estimation in complex stress-strein conditions under cyclic loadings. Strength of materials, N3, 1989

[4] L. B. Getsov, A. A. Nigin, M. G. Kabelevskiy: Use of finite-element method for numerical evaluation of thermal cycling endurance of disks. Strength of materials, N4, 1979, 17

[5] Cunningharn S. E., DeLuca D. P., Haake F. K.: Crack growth and life prediction in single crysta1 nickel Superalloys. Vol. I, WL-TR-94-4089, 1994

[6] Leverant G. A., Gell M.: The influence of temperature and cyclic frequency on the fatigue fracture of cube oriented nickel-base superalloy single crystal. Metall. Trans. A. 6 (**1975**), 367–371

[7] Telesman J., Ghosn L. J.: Fatigue Crack Growth Behavior of a PWA 1484 Single Crystal Superalloy at Elevated Temperatures. ASME Paper 95-GT-452, 1995

[8] Chan K. S., Feiger J., Lee Y.-D., John R., Hudak S. J.: Fatigue Crack Growth Thresholds of Deflected Mixed-Mode Cracks in PWA1484; Journal of Engineering Materials and Technology.127 (**2005**), 2–7

[9] Frost H. J., Ashby M. F.: Deformation- mechanism maps. 1982

[10] Report P&W. Dayton, 2005

[11] Shalin R. E., Svetlov I. L., Kachanov E. B. et al. Single crystals of nickel base superalloys. Machinery, 1997, 333

[12] Dulnev R. A., Svetlov I. L., Bychkov N. G. et al. Orientation dependence of thermal fatigue of nickel alloy single crystal; Strength problems (1988) 11, 3–9. (In Russian)

[13] A. I. Rybnikov, L. B. Getsov: New technique and results of thermal fatigue tests of superalloys and coatings; Proceedings of the sixth International congress on thermal stresses. Vienna, Austria, (**2005**) 1, 305–309

[14] Semenov A. S. PANTOCRATOR – Finite-element program specialized on the solution of non-linear problems of solid body mechanics; Proc. V-th Int. Conf. "Scientific and engineering problems of predicting the reliability and service life of structures and methods of their solution", St-Petersburg, 2003, 466-480

[15] Thermal strength of machine details. The theory. Experimental researches. Calculation. Editor Birger I. A. and Shorr B. F. Mechanical engineering, 1975 (In Russian)